Insight into Substrate Recognition by Urea-Based Helical Foldamer Catalysts Using a DFT Global Optimization Approach

Yaidel Toledo-González, Jean-Marc Sotiropoulos, Diane Bécart, Gilles Guichard, Philippe Carbonnière

JOC The Journal of Organic Chemistry

pubs.acs.org/joc Article

Insight into Substrate Recognition by Urea-Based Helical Foldamer Catalysts Using a DFT Global Optimization Approach

Yaidel Toledo-González,* Jean-Marc Sotiropoulos, Diane Bécart, Gilles Guichard, and Philippe Carbonnière*

Cite This: https://doi.org/10.1021/acs.joc.2c00562 Read Online

ACCESS | Metrics & More | Article Recommendations | Supporting Information

ABSTRACT: Peptides and foldamers have recently gained increasing attention as chiral catalysts to achieve challenging (asymmetric) transformations. We previously reported that short helically folded aliphatic oligoureas in combination with achiral Brønsted bases are effective H-bonding catalysts for C−C bond-forming reactions—i.e., the conjugate addition of 1,3-dicarbonyl pronucleophiles to nitroalkenes—with high reactivity and selectivity and at remarkably low chiral catalyst/substrate molar ratios. This theoretical investigation at the density functional theory level of theory, aims to both analyze how the substrates of the reaction interact with the foldamer catalyst and rationalize a chain-length dependence effect on the catalytic properties. We confirm that the first two ureas are the only H-bond donors available to interact with external molecules. Moreover, each urea site interacts with one of the two reactants allowing a short distance between the two reacting carbons, thus facilitating the conjugated addition. Additionally, it was observed that the molecular recognition and catalyst−substrate interactions are mainly governed by electrostatic interactions but not orbital interactions (see from NBO if this is finally true). On these grounds, an electrostatic potential (ESP) analysis showed an important internal charge separation in the catalyst, the positive ESP region being concentrated around the first two ureas, with its area extending as the number of residues increases.

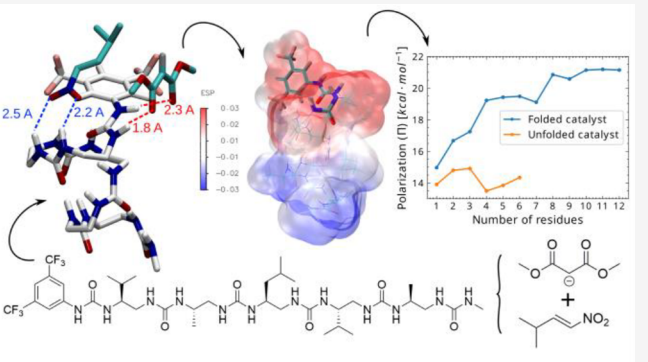

INTRODUCTION

Defined sequences and folding (e.g., protein tertiary structure) are two of the main attributes of biopolymers that determine their specific and highly diverse functionalities (transport, sensing, signaling, energy storage, catalysis, ...). In enzymes, precise organization of active-site side chains in the 3D space, participation of cofactors, and electrostatic interactions are inherent elements mediated by a folded yet dynamic backbone which contributes to facilitating the interaction with the substrate and stabilizing the transition states, ultimately leading to catalytic activity.[1,2] Inspired by protein structures, small- and medium-size synthetic folded strands have received increasing interest as chiral catalysts because, on the one hand, they are modular and scalable and, on the other hand, they may retain some key features of enzymes such as high reactivity and stereoselectivity but also chemoselectivity and site-selectivity. This is particularly true for synthetic α-peptides which were found to be well-suited as chiral catalysts for a broad range of asymmetric transformations.[3−6] Concurrently, foldamers—non natural oligomers with defined folding patterns—which exhibit both sequence tunability and folding predictability, have gained increasing interest as scaffolds for catalyst design.[7] In these systems, the active site generally consists of an array of spatially arranged functional side chains and can also involve main-chain functional groups well-organized through folding. This is the case for chiral aliphatic N,N′-linked oligoureas, a class of helical foldamers previously reported to catalyze enantioselective C−C bond-forming reactions, in which main chain (thio)urea NH groups located at the positive pole of the helix macrodipole are available to bind and activate substrates.[8,9] This system actually shows similarities with the well-studied helical polypeptides developed as catalysts for Juliá−Colonna epoxidations in which the four N-terminal amide NH groups not engaged in intramolecular H-bonds are involved as H-bond donor groups with the substrates.[10,11]

Oligourea hexamer **1**, which contains seven urea linkages (Figure 1), was found to catalyze the conjugate addition of 1,3-dicarbonyl substrates to nitroalkenes in high yield and enantioselectivity at remarkably low catalyst/substrate molar ratios in the presence of an achiral Brønsted base such as Et_3N or DIPEA.[9] In this paper, it was observed that the chain length of the foldamer was a crucial parameter in terms of reactivity and enantiocontrol. Whereas the helically folded 6-residue long

Received: April 20, 2022

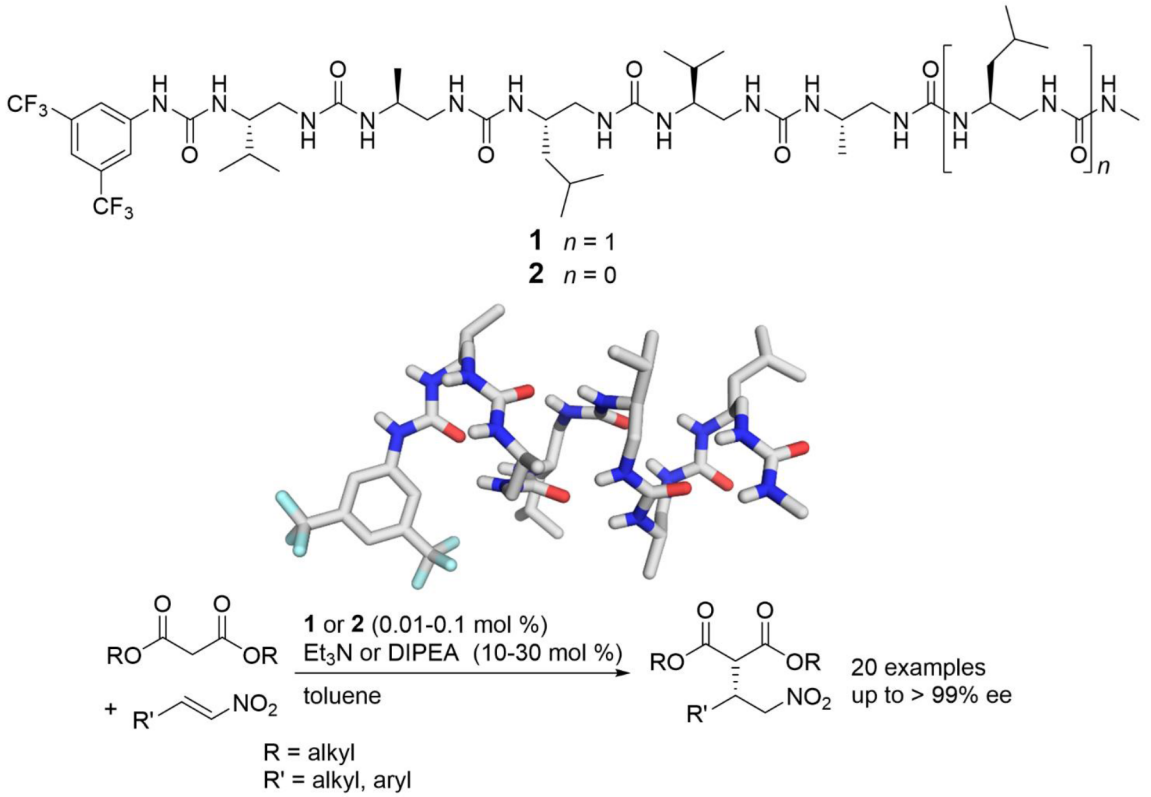

Figure 1. Formulas of helical foldamers **1** and **2**, X-ray structure of **1**, and their use as H-bond donor chiral catalysts in the enantioselective conjugate addition of 1,3-dicarbonyl compounds to nitroalkenes.[9]

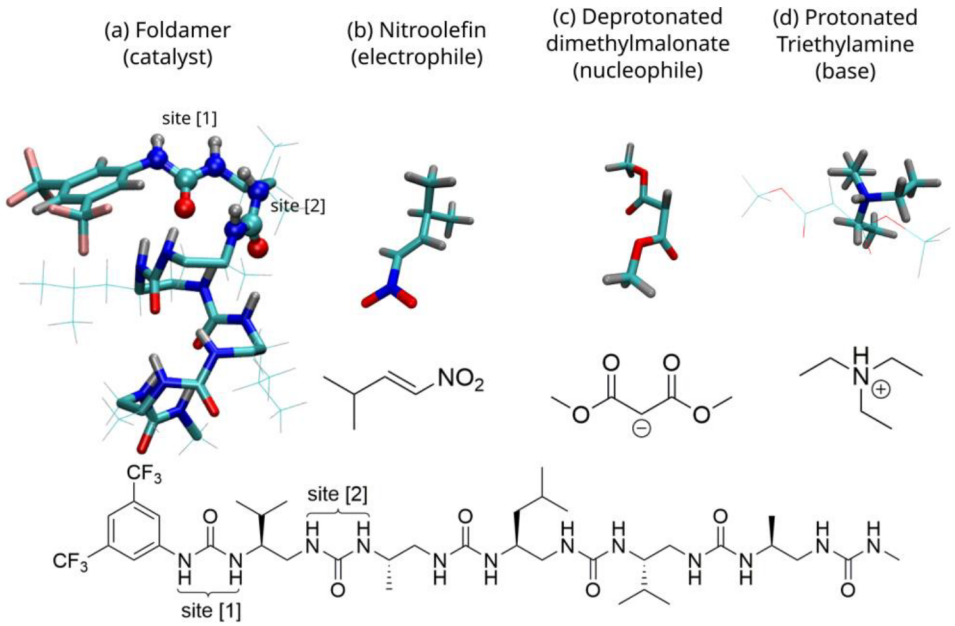

Figure 2. (a) Structure of the foldamer-based chiral catalyst (hexaurea **2**). The studied reaction involves the (1*E*)-3-methyl-1-nitrobut-1-ene as nitroolefin (b) and the deprotonated dimethylmalonate (c), the last being deprotonated by the triethylamine (d).

oligourea (1) and the related 5-mer (2) show remarkable catalytic properties, oligomers with shorter chain lengths were much less effective in terms of enantiocontrol. Structure–activity relationship studies further confirmed that the helix conformation of the oligourea foldamer is a major determinant of their catalytic activities and that the second (thio)urea site is as important as the first. Related hybrid oligomers consisting of a short oligourea segments fused at the N-terminus of a short helical peptide have also been used to catalyze similar reactions.[12−14]

Mono- and bis(thio)urea H-bond donor catalysts[15−23] have been studied extensively, and in many cases, detailed computational investigations have been conducted on these small molecules to explore the catalytic processes at the

https://doi.org/10.1021/acs.joc.2c00562
J. Org. Chem. XXXX, XXX, XXX−XXX

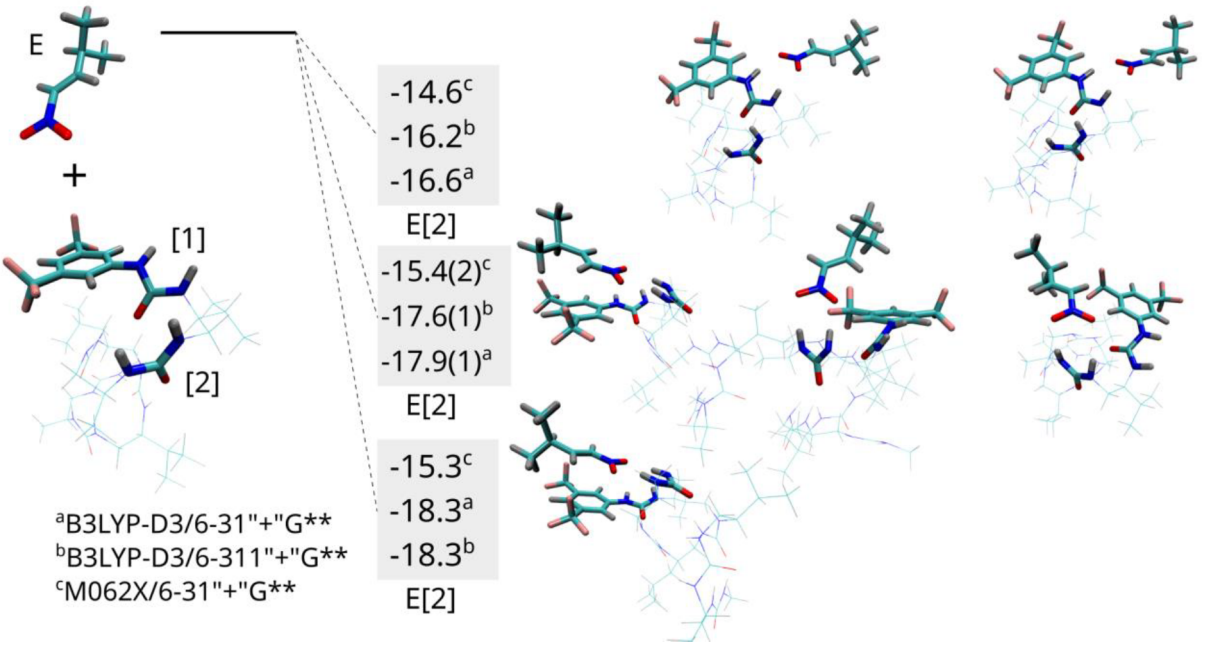

Figure 3. Binding energies (in kcal/mol) of the nitroalkene (electrophile) on the hexaurea catalyst **2**. Here [1] and [2] represent the two binding sites of the catalyst.

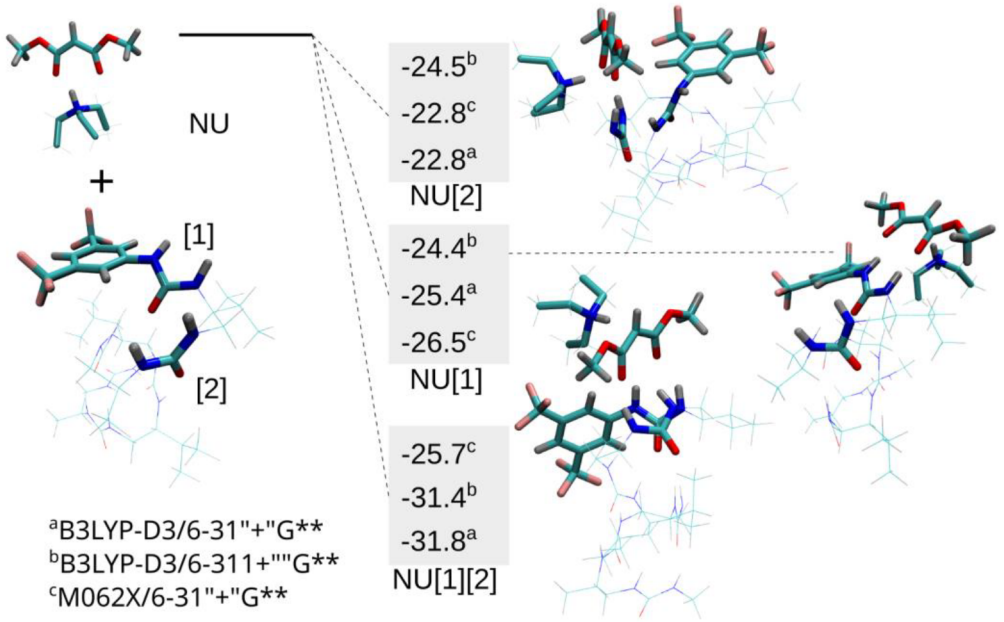

Figure 4. Binding energies (in kcal/mol) of the deprotonated malonate (nucleophile) on the hexaurea catalyst **2**. Here [1] and [2] represent the two binding sites of the catalyst.

atomistic level, mainly by finding the related transitions states.[20−22,24−30] In contrast, the mechanism of synergistic activation with oligourea foldamer-based catalysts has not yet been investigated from a theoretical point of view. Our aim in this work was thus to use computational chemistry to study the binary system composed of chiral H−bond donor foldamer catalyst/achiral Brønsted base, by asking the following questions: What kind of interactions occur between the reactants and the foldamer catalyst? What is the role of the helical shape in the catalytic process? Which is the influence of the catalyst on the capability of the reactants to react? To that end, the properties of the foldamer catalyst as a function of its chain length, as well as the interactions between the catalyst and reaction substrates, were carefully investigated at the DFT level of theory.

RESULTS AND DISCUSSION

Molecular Recognition. The global optimization search, which involves the helical foldamer, both reactants ((1*E*)-3-methyl-1-nitrobut-1-ene as electrophile and deprotonated dmiethylmalonate as nucleophile), and the achiral base (triethylamine), was first performed using **2** (5-residues long oligomer) as reference because it requires less computational time compared to **1** (Figure 2). As depicted in Figures 3 and 4,

https://doi.org/10.1021/acs.joc.2c00562
J. Org. Chem. XXXX, XXX, XXX−XXX

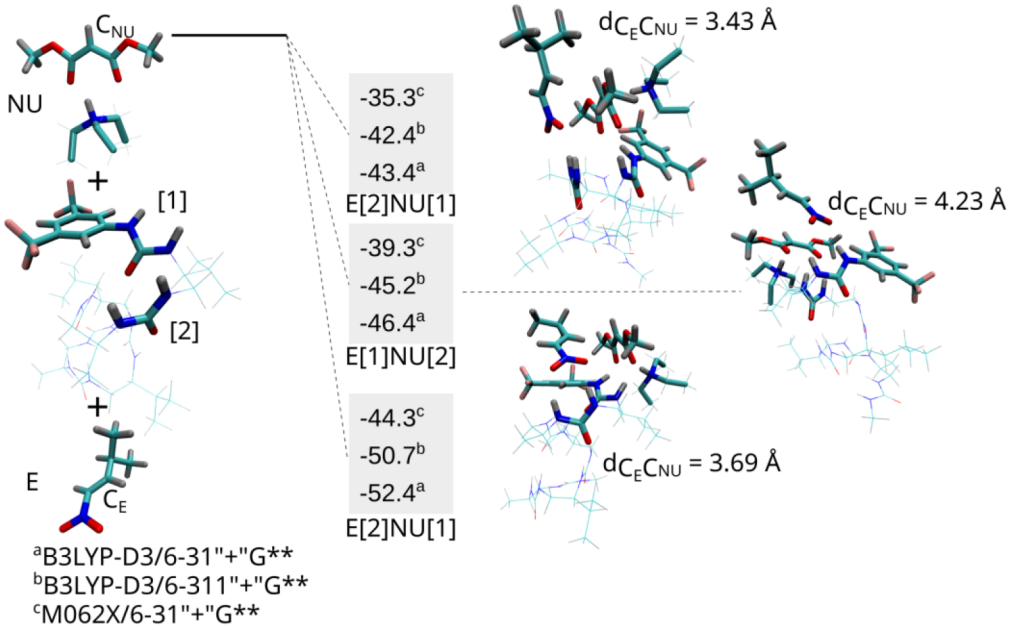

Figure 5. Binding energies (in kcal/mol) of the deprotonated malonate (nucleophile) and the nitroalkene (electrophile) on the hexaurea catalyst **2**. Here [1] and [2] represent the two binding sites of the catalyst.

which show the most energetically stable conformers, this numerical process found that only the two first urea groups (denoted as site [1] and [2] in the figures) can accommodate the reactants.

Among the possible configurations, the site [2] is generally more favorable for the electrophilic species ((1*E*)-3-methyl-1-nitrobut-1-ene) and leads to a stabilization of about 18 kcal/mol (Figure 3) while the nucleophilic species (deprotonated dimethylmalonate) tends to be astride on the two sites with a stabilization of about 31 kcal/mol (Figure 4). However, when the two reactants are considered together for binding on the foldamer, the nucleophilic species appears to bind clearly and exclusively on site [1], as stated in Figure 5. This clearly reveals a bifunctional activation of the catalyst from the two first sites.

The four structures of Figure 5 were obtained (i) by considering the most stable situation of Figure 4 (nucleophile in astride position) in which the nucleophile species was placed on sites [1] and [2] and (ii) by considering the most stable structure of Figure 3 in which the electrophilic species binds on site [2]. When the electrophile is placed in the vicinity of site [2], it is then observed that the nucleophile moves from the astride position to site [1] during the local optimization process. Note that the three-model chemistry used revealed the same pattern: the B3LYP-D3 results overbound for few kcal/mol with respect to their M06-2X counterparts, and no sensitive deviations are found with the use of a triple-ζ basis set. Moreover, our computations show that the deprotonation of the malonate by the achiral base is sensitively favored in the presence of the catalyst at 300 K (see the Supporting Information, Figure S1). Overall, these results are consistent with experimental ^{1}H NMR data of **1a** obtained upon successive addition of malonate, triethylamine, and nitrostyrene (see Figures S4−S8 in the Supporting Information) showing that under the conditions used (for solubility issues, spectra were recorded in a mixture of acetonitrile-d_3/DMSO-d_6 (88:12 v/v)) (i) the deprotonated malonate interacts with the catalyst, more than the cognate malonate, (ii) this interaction involves site [1], and (iii) triethylamine critically controls the interaction process because nitrostyrene and malonate alone do not lead to significant modification of the spectrum of **1a**.

Furthermore, one can note that the most energetically favored structural position may also, from a structural point of view, favor a C−C bond formation reaction between the two reactants since the corresponding C−C distance for this optimized structure is calculated at 3.69 Å.

Finally, a few points on the methodology used for the computation of binding energies: (i) Basis Set Superposition Error (BSSE) was found not to influence the reported binding energies, and (ii) the role of the diffuse functions was identified as fundamental to describe these systems (see the section "Influence of BSSE and diffuse function in our computations" in the Supporting Information for more details).

Nature of the Binding Interactions. We next wondered about the nature of the stabilizing interactions between the reactant and the catalyst, i.e., whether the interactions are more orbital or electrostatic in nature.

Concerning the investigation of the orbital interactions and according to the Frontier Orbital Theory,[31] the energies of the HOMO of each of the substrates were compared to those of the LUMO of the oligourea foldamer electron acceptor (see the Supporting Information for the description of the molecular orbitals, Figure S2). A $HOMO_{(substrates)}$−$LUMO_{(catalyst)}$ energy gap of about 3.5 and 6 eV is observed for the malonate and the nitroalkene, respectively. This value is not sensitively modified by the number of the residues of the foldamer (from monomer to hexamer) as shown in Figure S2, thus suggesting that the change of affinity between the substrates and the foldamer with respect to the number of residues is not governed by orbital interactions. Although donor orbitals of the substrates and acceptor orbitals of the catalyst are quite far in terms of energy observed (not depicted in the Supporting Information), a very small mixing between the orbitals of the two kinds cannot be ignored since the decrease of each HOMO energy of the substrates when

https://doi.org/10.1021/acs.joc.2c00562
J. Org. Chem. XXXX, XXX, XXX−XXX

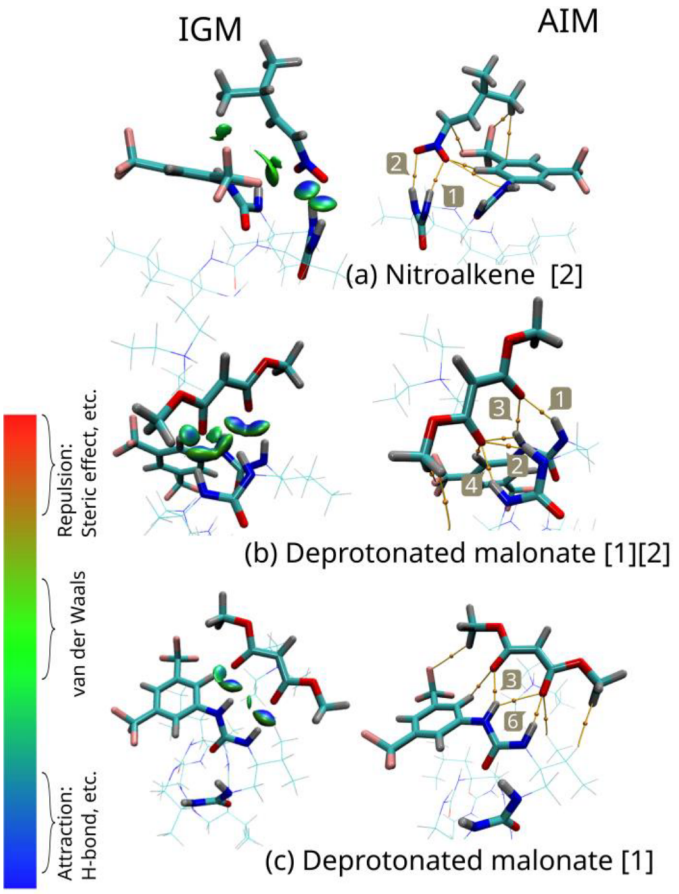

	BCP	Type	E $[kcal/mol]$
1	O···H − N	H-bond	-3.1323
2	O···H − N	H-bond	-2.7344
...	...	vdW	-

	BCP	Type	E $[kcal/mol]$
1	O···H − N	H-bond	-4.1871
2	O···H − N	H-bond	-3.4733
3	O···H − N	H-bond	-4.4558
4	O···H − N	H-bond	-4.5240
...	...	vdW	-
7	O···H − C	H-bond	-2.5617
...	...	vdW	-

	BCP	Type	E $[kcal/mol]$
...	...	vdW	-
3	O···H − N	H-bond	-4.4750
...	...	vdW	-
6	O···H − N	H-bond	-5.7373
...	...	vdW	-

	BCP	Type	E^a $[kcal/mol]$	E^c $[kcal/mol]$
...	...	VdW	-	-
8	O ··· H-N	H-bond	−4.2368	−3.1358
...	...	VdW	-	-
11	O ··· H-N	weak H-bond	−1.8705	−2.5600
12	O ··· H-N	H-bond	−2.9037	−2.0391
13	O ··· H-N	H-bond	−5.8691	−5.3398
14	O ··· H-N	H-bond	−3.8118	−2.0632
$12(O) - 14(H)$	O ··· H-N	H-bond	-	−2.5556

[a]B3LYP-D3/6-31"+"G(d,p)
[c]M062X/6-31"+"G(d,p)

Figure 6. Noncovalent interactions in the most stable conformations found for the hexaurea foldamer **2** interacting with the substrates. In the tables, BCP stands for "Bond Critical Point" as defined by QTAIM theory and vdW stands for "van der Waals interactions". The value E reported is an estimation of the binding energy related to that H-Bond[32] (see section "Non-covalent interactions" in the Supporting Information for more details on the computation and meaning of E). Unless otherwise specified, the values were obtained with B3LYP-D3/6-31"+"G(d,p).

connected to the foldamer is about 0.45 eV. This decrease is constant whatever the number of residues of the foldamer.

Figure 6 illustrates the noncovalent interactions between the foldamer and the different substrates obtained by Integrated Gradient Model (IGM) and Atom in Molecules (QTAIM) methods (see the Supporting Information for more details on these methods, section "Non-covalent interactions"). Four complexes were considered: (a) the most stable structure of the nitroalkene on the catalyst, binding on site [2]; (b) the most stable structure of the deprotonated malonate on the catalyst, astride on sites [1] and [2]; (c) the second most stable structure of the deprotonated malonate, binding on site [1]; and (d) the most stable structure of the nitroalkene binding on site [2] and the malonate binding on site [1].

The nitroalkene was found to bind to site [2] by means of two H-bonds, while a region of van der Waals interactions rises around the 3,5-bis(trifluoromethyl)phenyl group (see Figure 6a). Differently, the malonate ester binds to the catalyst exclusively using an array of H-bonds, i.e., five for the complex shown in Figure 6b and two for the complex shown in Figure 6c. In any case, it is observed that the average interaction energy by the hydrogen bond is about 4 kcal/mol, which is relatively strong and would have predominantly an electrostatic nature (see computations and AIM details in the section "Non-covalent interactions" of the Supporting Information for more details), as generally observed in biomolecules.[33] The results obtained with M06-2X were equivalent (see Figure 6d).

To evaluate the stabilization energy due to orbital interactions, a Second Order Perturbation Theory Analysis of Fock Matrix in NBO Basis was carried out in the 3-mer (which gives low selectivity[9]), 5-mer (which gives high selectivity[9]), and 9-mer foldamers (which has not been studied

https://doi.org/10.1021/acs.joc.2c00562
J. Org. Chem. XXXX, XXX, XXX−XXX

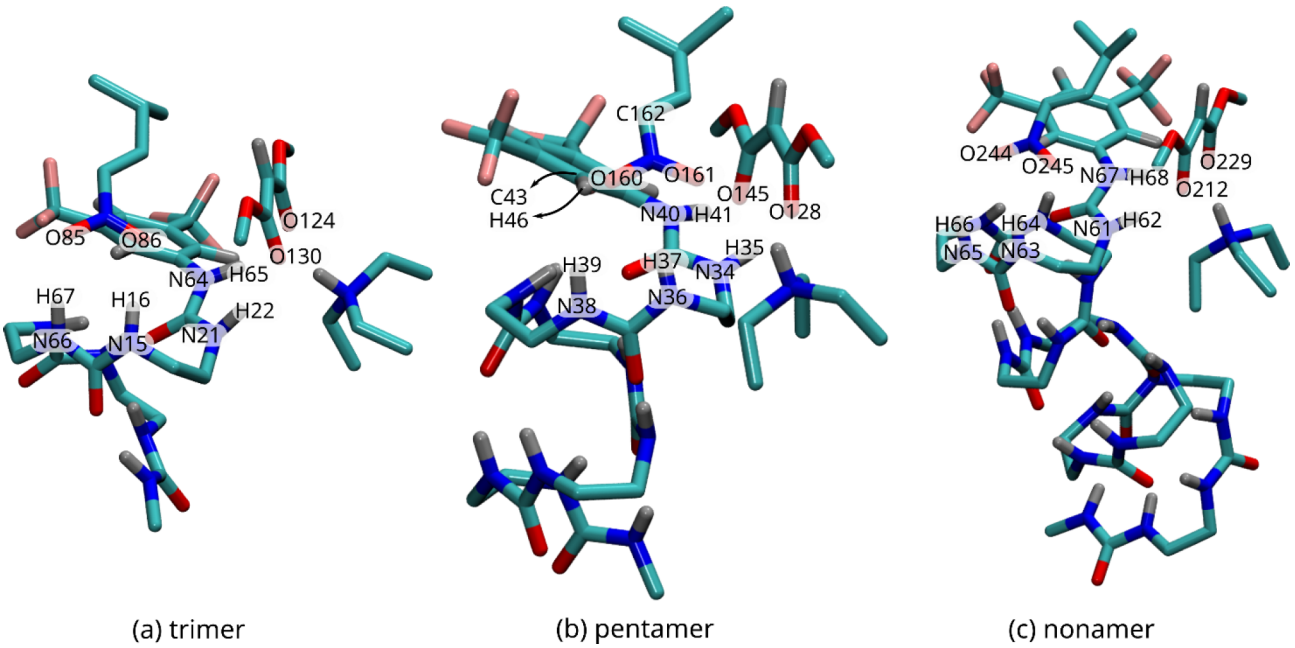

Figure 7. Numbering of the atoms involved in the NBO analysis.

experimentally yet) interacting with both substrates (see Figure 7 and Table 1). It is observed that the stabilizing interactions between the substrates and the foldamer are similar in the three systems, with two exceptions localized in the trimer: O86 to N15−H16 and O124 to N64−H65, which are ∼4 kcal/mol and ∼3 kcal/mol higher than their corresponding values in the pentamer and nonamer, respectively. Disregarding those two exceptions, only one interaction has a considerable stabilization energy due to orbital interactions in the three systems, and it is localized in one of the two acceptor dimethylmalonate's oxygen (see, for example, the interaction between O128 and N34−H35 in the pentamer of Figure 7b). Furthermore, it is interesting to point out that the stabilizing interactions are constant and do not depend on the catalyst's length.

Table 1. Second-Order Perturbation Theory Analysis of Fock Matrix in NBO Basis for the 3-mer, 5-mer, and 9-mer Foldamers Represented in Figure 7[a]

donor (i)	type	acceptor (j)	type	$E(2)$ (kcal/mol)
		Trimer		
O85	LP(2)	N66−H67	BD*(1)	3.56
O85	LP(2)	N15−H16	BD*(1)	0.22
O86	LP(2)	N15−H16	BD*(1)	7.14
O124	LP(2)	N64−H65	BD*(1)	4.15
O130	LP(1)	N21−H22	BD*(1)	9.23
		Pentamer		
C43−H46	BD(1)	O160	LP(3)	0.12
O160	LP(1)	N38−H39	BD*(1)	0.93
O160	LP(2)	N36−H37	BD*(1)	2.54
O161	LP(2)	N36−H37	BD*(1)	3.06
O145	LP(2)	N40−H41	BD*(1)	1.94
O128	LP(1)	N34−H35	BD*(1)	10.26
		Nonamer		
O244	LP(1)	N65−H66	BD*(1)	0.75
O244	LP(2)	N63−H64	BD*(1)	3.01
O245	LP(2)	N63−H64	BD*(1)	2.85
O229	LP(2)	N67−H68	BD*(1)	1.88
O212	LP(1)	N61−H62	BD*(1)	10.50

[a] $E(2)$ is the energy of hyper conjugative interaction (stabilization energy), LP stands for lone pair, BD stands for bond, and RY stands for Rydberg (all related to the NBO nomenclature).

Reactive Behavior. The theoretical estimation of the strength of the electrophile and nucleophile interaction with the foldamer and stabilization of charged intermediates arises from the evaluation of the electrostatic potential and some quantities statistically related to it[34] (see the Supporting Information for more details, section "Electrostatic Interactions"). The ESP surfaces of the foldamers as a function of their chain length (monomer, dimer, hexamer, and dodecamer) and their unfolded form are shown in Figure 8. A set of indexes that illustrates the reactivity of the catalyst with respect to the number of its residues is also reported: (i) the index of polarization (Π) which is the internal charge separation within the molecule and is related to its dipole moment (Figure 8g), (ii) the minimum and maximum value of the ESP (Figure 8h), and (iii) the sigma indexes (σ^2_{tot}) that are used as indicators of the tendency of the molecule to interact by its positive (σ^2_+) or its negative (σ^2_-) region (Figure 8.i). From Figure 8, it is clearly seen that the polarization increase with the number of residues when the catalyst is folded, while in the unfolded state it remains nearly constant and weaker (see Figure 8g). The polarization difference in each case is directly related to the intramolecular H-bonding cooperation between ureas, which is present in the folded catalyst but not in the unfolded form. This reveals the importance of the helical conformation. Figure 8g also reveals three ranges of internal charge separation: (i) from monomer to trimer in which the positive region of the ESP surfaces encloses partially the binding sites [1] and [2], (ii) from tetramer to heptamer for which the positive region fully enclose the binding sites and the polarization is slightly higher, (iii) from octamer to dodecamer for which the positive ESP region extends further outside the two reactive sites. Furthermore, the maximum value of the positive charge (see Figure 8h) which is centered on site [1] increases form the

https://doi.org/10.1021/acs.joc.2c00562
J. Org. Chem. XXXX, XXX, XXX−XXX

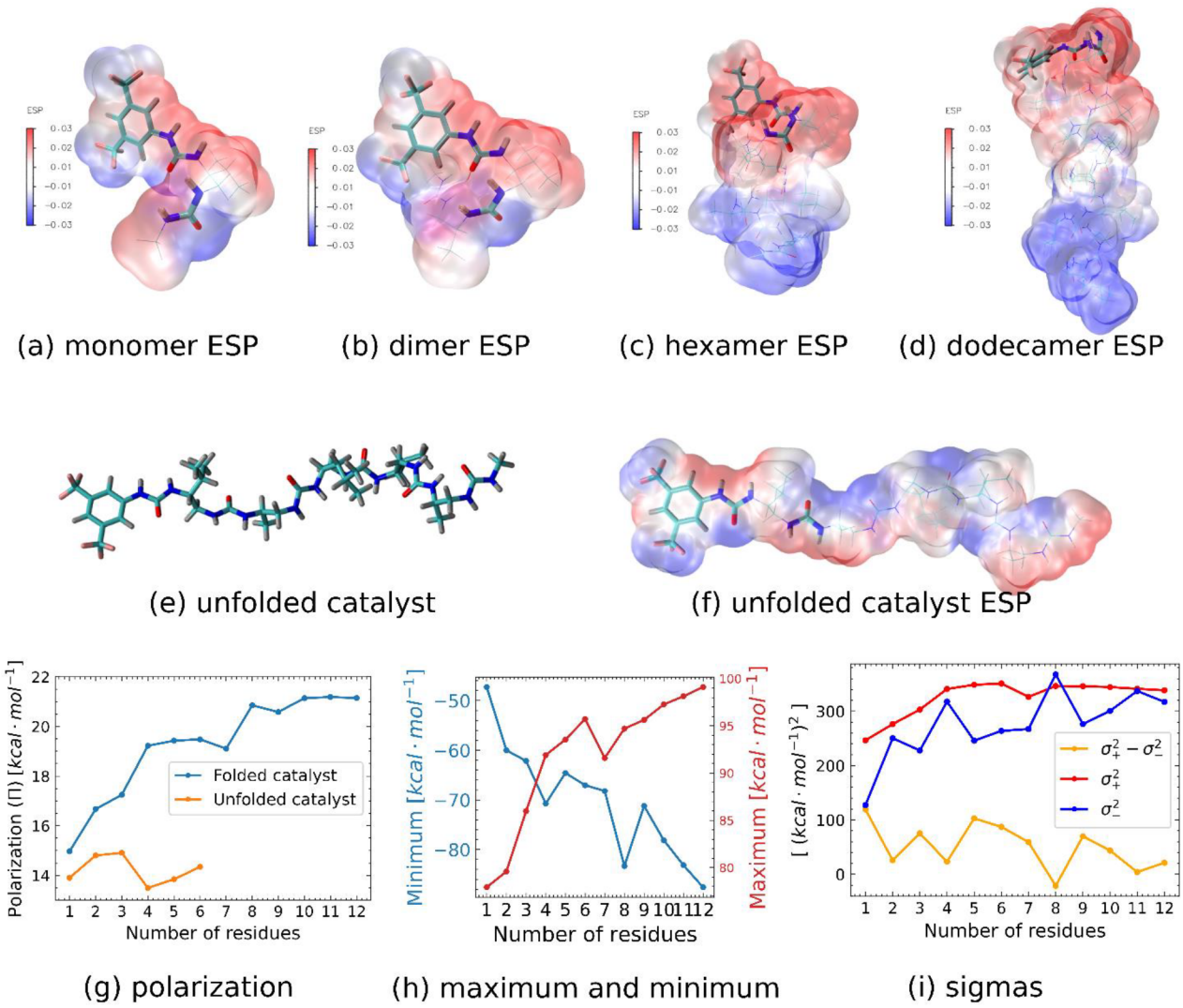

Figure 8. Catalyst electrostatic potential and related properties. (a–d) ESP surfaces of various folded catalysts with different chain lengths. (e,f) Hexaurea **2** unfolded. (g–i) Interesting ESP statistically based quantities for the folded molecule and for the unfolded oligomer when specified (see the Supporting Information for more information on these statistically based quantities, section "Electrostatic interactions").

monomer to dodecamer. About 70% of the gain is reached for the tetrameric form and beyond in the series. This shows that the electron acceptor character of the foldamer increases with the number of residues and seems to extend beyond the site [1] and two [2] for oligomers larger than the heptameric form (see the red line in Figure 8i).

HOMO–LUMO Gap of the Reactants. According to Frontier orbital theory,[31] the reactivity between an electrophile and a nucleophile is governed by the HOMO–LUMO gap of the overall system. On that point, Figure 9 illustrates the evolution of the HOMO–LUMO gap with respect to the number of the residues when the reactants bind to the catalyst.

It is clearly seen that the gap significantly decreases with the introduction of the catalyst in the system, from 5.21 to 2.74 eV, and then it becomes nearly constant from monomer to dodecamer. This suggests two important points (at least): first, the presence of the 1-mer catalyst considerably lowers the HOMO–LUMO gap between the substrates, facilitating the reaction, and second, the changes in reactivity and enantioselectivity observed in the experiment,[9] which are dependent on the catalyst's size, should not be related to its

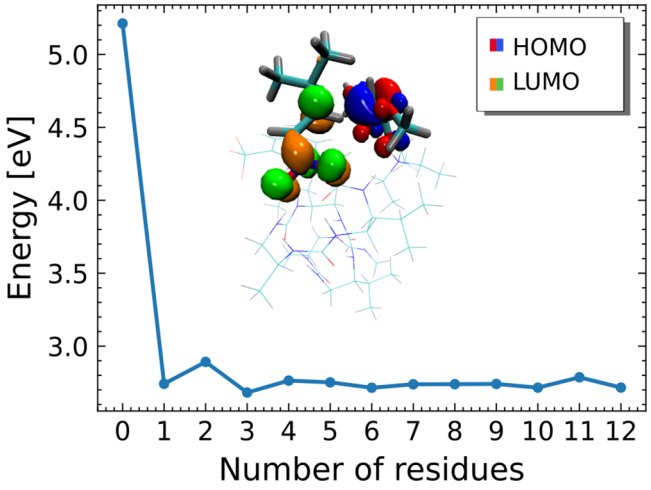

Figure 9. HOMO–LUMO gap behavior in the substrates as a function of the catalyst chain length. HOMO was calculated for the deprotonated malonate ester (nucleophilic species) and LUMO for the nitroalkene (electrophillic species).

https://doi.org/10.1021/acs.joc.2c00562
J. Org. Chem. XXXX, XXX, XXX–XXX

influence on the frontier orbitals of the substrates positioned this way, as their gap is constant no matter the foldamer's number of residues.

CONCLUSIONS

We reported here the first computational insights into the molecular recognition and catalytic properties of aliphatic N,N′-linked oligoureas (foldamers) which together with achiral Brønsted base catalyze the addition of malonate to nitroolefins at low loading (0.01−0.1 mol % in chiral catalyst). The present work reveals that the foldamer interacts with and activates simultaneously both reactants and not only the electrophile (nitroalkene) as could have been anticipated when designing this synergistic catalytic system. This computational analysis shows that the nitroalkene is bound to the second site, whereas the malonate ester is located at the first site, the two substrates being engaged in multiple H-bond interactions.

Orbital and electrostatic interaction are of equivalent magnitude, but only the latter evolves with the size of the foldamer: the polarization of the foldamer was observed to increase due to the internal urea−urea cooperation resulting from the helix conformation.

Finally, our analysis reveals that the reactivity of the reactants should increase in the presence of the catalyst as the difference between the highest occupied molecular orbital of the nucleophile (malonate) and the lowest unoccupied molecular orbital of the electrophile (nitroalkene) decreases by 2.47 eV when the catalyst is added and is place in a better suited position for the reaction to take place.

Overall, these results open the possibility of further designs and improvements useful for expanding the scope of foldamer-catalyzed reactions. In this respect, molecular modeling of the energetic profile from localization of the corresponding transition states to estimate the enantiocontrol of the C−C bond-forming reaction between nitroalkene and malonate in the presence of (thio)urea foldamer catalyst as a function of its chain-length is still needed and will be reported in due course.

COMPUTATIONAL METHODS

The heptaurea (6-mer) was optimized from the experimental X-ray structures (CCDC accession code 1534525).[9] Starting with this 6-mer, the other structures were deduced as follows: from the heptaurea, we removed one residue at a time and optimized the resulting structure, obtaining in this way the hexaurea (5-mer, **2**), pentaurea (4-mer), and so on. We then duplicated the backbone of the heptaurea and connected the two resulting helices to generate the 12-mer molecule. Finally, we followed the previously mentioned procedure of removing residues one by one and optimizing until we obtained the octaurea (7-mer), completing in this way a set of 12 foldamers (see Figure S3 of the Supporting Information for their formulas).

The most stable binding sites were found from Global Optimization procedures.[35] Some additional possible conformers were found from the most stable species previously obtained. Molecular geometry optimizations were performed with the Gaussian 16 Revision C.01 software[36] using DFT[37−40] with the B3LYP-D3 functional[41−46] and 6-31G(d,p) basis set.[47] Additionally, a diffuse function[48] was specified for O, N, F, and the negative charged carbon of the malonate anion atoms (hereafter 6-31"+"G(d,p)). The SMD variation of the Polarizable Continuum Model (PCM) using the integral equation formalism variant (IEFPCM) solvent model[49] was set in all the optimizations with toluene and Solvent Accesible Surface (SAS) representing the solute−solvent boundary. The temperature in all simulations was set to 298.15 K, in agreement with the experiments.

The lowest energy structures of the systems composed of the malonate (i.e., dimethyl malonate) and/or nitroalkene (i.e., (1*E*)-3-methyl-1-nitrobut-1-ene) binding onto the hexaurea catalyst **2**[9] were obtained by the Global Search Algorithm of Minima (GSAM) (see ref 50 and references cited therein) interfaced with the Gaussian16 program[36] for computations of the energies and gradients. The GSAM procedure consists of a random process of structure generation followed by an iterative process. For each iteration, the structures are partially optimized (typically 30 cycles of optimization) and sorted from their relative energy with respect to the most stable structure of the set and refined from their topological differences. Generally, the iterative process consists of four steps in which the relative energetic criterion that selects the structures for the next step is successively tightened, typically from 100 to 20 kcal/mol. This allows us to decrease by 30−60% the number of the structures for the next step of optimization. The final structures are then fully optimized. Our choice to apply the B3LYP-D3 functional, together with the 6-31"+"G(d,p) basis set, stems from our previous experience, which showed that this combination leads to good agreement between experimental and theoretical vibrational spectra of different types of hydrates[51,52] and structure of micro hydrated nucleic acid basis.[53] Nevertheless, regarding the effect of basis sets,[54] functionals,[55] and the estimation of interatomic molecular interactions by DFT, all of the energies of the low-lying isomers reported in the present manuscript were fully reoptimized with the B3LYP-D3/6-311"+"G(d,p) and M06-2X/6-31"+"G(d,p) model chemistry.

Moreover IGM[56] and QTAIM[57−59] analyses were performed with Multiwfn[60] software, while NBO[61−68] analysis was perform with Gaussian software.

ASSOCIATED CONTENT

Supporting Information

The Supporting Information is available free of charge at https://pubs.acs.org/doi/10.1021/acs.joc.2c00562.

Some deeper annotations in some theoretical quantities and methods used; Figures S1−S3 further support the description of the systems; Figures S4−S8 show related NMR experimental results (PDF)

AUTHOR INFORMATION

Corresponding Authors

Yaidel Toledo-González − *Université de Pau et des Pays de l'Adour, E2S UPPA, CNRS, IPREM, 5254 Pau, France;* orcid.org/0000-0001-7349-8143; Email: ytgonzalez@univ-pau.fr

Philippe Carbonnière − *Université de Pau et des Pays de l'Adour, E2S UPPA, CNRS, IPREM, 5254 Pau, France;* orcid.org/0000-0003-0305-3231; Email: philippe.carbonniere@univ-pau.fr

Authors

Jean-Marc Sotiropoulos − *Université de Pau et des Pays de l'Adour, E2S UPPA, CNRS, IPREM, 5254 Pau, France*

https://doi.org/10.1021/acs.joc.2c00562
J. Org. Chem. XXXX, XXX, XXX−XXX

Diane Bécart − *Université Bordeaux, CNRS, Bordeaux INP, CBMN, UMR 5248, Institut Européen de Chimie et Biologie, F-33607 Pessac, France*

Gilles Guichard − *Université Bordeaux, CNRS, Bordeaux INP, CBMN, UMR 5248, Institut Européen de Chimie et Biologie, F-33607 Pessac, France;* orcid.org/0000-0002-2584-7502

Complete contact information is available at: https://pubs.acs.org/10.1021/acs.joc.2c00562

Notes

The authors declare no competing financial interest.

■ ACKNOWLEDGMENTS

The authors acknowledge financial support from the ANR (Project HCO_for_LLAC ANR-18-CE07-0018). This work was also granted access to the HPC resources of TGCC Irene-Rome under the allocation A0110813033 made by GENCI. A predoctoral fellowship from the IDEX of Univ. Bordeaux to D.B. is gratefully acknowledged (funding from the French National Research Agency - Program ANR No. 10-IDEX-03-02).

■ REFERENCES

(1) Drauz, K, Gröger, H, May, O. *Enzyme Catalysis in Organic Synthesis*, 3 Volume Set; John Wiley & Sons, 2012; 2143 p.

(2) Agarwal, P. K. A Biophysical Perspective on Enzyme Catalysis. *Biochemistry.* **2019**, *58*, 438−49.

(3) Davie, E. A. C.; Mennen, S. M.; Xu, Y.; Miller, S. J. Asymmetric Catalysis Mediated by Synthetic Peptides. *Chem. Rev.* **2007**, *107*, 5759−812.

(4) Metrano, A. J.; Chinn, A. J.; Shugrue, C. R.; Stone, E. A.; Kim, B.; Miller, S. J. Asymmetric Catalysis Mediated by Synthetic Peptides, Version 2.0: Expansion of Scope and Mechanisms. *Chem. Rev.* **2020**, *120*, 11479−615.

(5) Lewandowski, B.; Wennemers, H. Asymmetric catalysis with short-chain peptides. *Curr. Opin Chem. Biol.* **2014**, *22*, 40−6.

(6) Akagawa, K.; Kudo, K. Development of Selective Peptide Catalysts with Secondary Structural Frameworks. *Acc. Chem. Res.* **2017**, *50*, 2429−39.

(7) Girvin, Z. C.; Gellman, S. H.; Foldamer; Catalysis. *J. Am. Chem. Soc.* **2020**, *142*, 17211−23.

(8) Diemer, V.; Fischer, L.; Kauffmann, B.; Guichard, G. Anion Recognition by Aliphatic Helical Oligoureas. *Chem. − Eur. J.* **2016**, *22*, 15684−92.

(9) Bécart, D.; Diemer, V.; Salaün, A.; Oiarbide, M.; Nelli, Y. R.; Kauffmann, B.; et al. Helical Oligourea Foldamers as Powerful Hydrogen Bonding Catalysts for Enantioselective C−C Bond-Forming Reactions. *J. Am. Chem. Soc.* **2017**, *139*, 12524−32.

(10) Kelly, D. R.; Roberts, S. M. The mechanism of polyleucine catalysed asymmetric epoxidation. *Chem. Commun.* **2004**, 2018−20.

(11) Colonna, S.; Perdicchia, D.; Mauro, E. D. Enantioselective reactions catalyzed by synthetic enzymes. A model for chemical evolution. *Tetrahedron Asymmetry.* **2009**, *20*, 1709−14.

(12) Fremaux, J.; Mauran, L.; Pulka-Ziach, K.; Kauffmann, B.; Odaert, B.; Guichard, G. α-Peptide−Oligourea Chimeras: Stabilization of Short α-Helices by Non-Peptide Helical Foldamers. *Angew. Chem. Int. Ed.* **2015**, *127*, 9954−8.

(13) Le Bailly, B. A. F.; Byrne, L.; Clayden, J. Refoldable Foldamers: Global Conformational Switching by Deletion or Insertion of a Single Hydrogen Bond. *Angew. Chem. Int. Ed.* **2016**, *55*, 2132−6.

(14) Sato, K.; Umeno, T.; Ueda, A.; Kato, T.; Doi, M.; Tanaka, M. Asymmetric 1,4-Addition Reactions Catalyzed by N-Terminal Thiourea-Modified Helical L -Leu Peptide with Cyclic Amino Acids. *Chem. − Eur. J.* **2021**, *27*, 11216−20.

(15) Takemoto, Y. Recognition and activation by ureas and thioureas: stereoselective reactions using ureas and thioureas as hydrogen-bonding donors. *Org. Biomol Chem.* **2005**, *3*, 4299−306.

(16) Doyle, A. G.; Jacobsen, E. N. Small-Molecule H-Bond Donors in Asymmetric Catalysis. *Chem. Rev.* **2007**, *107*, 5713−43.

(17) Jones, C. R.; Dan Pantoş, G.; Morrison, A. J.; Smith, M. D. Plagiarizing Proteins: Enhancing Efficiency in Asymmetric Hydrogen-Bonding Catalysis through Positive Cooperativity. *Angew. Chem. Int. Ed.* **2009**, *48*, 7391−4.

(18) Crespo-Peña, A.; Monge, D.; Martín-Zamora, E.; Álvarez, E.; Fernández, R.; Lassaletta, J. M. Asymmetric Formal Carbonyl-Ene Reactions of Formaldehyde *tert* -Butyl Hydrazone with α-Keto Esters: Dual Activation by Bis-urea Catalysts. *J. Am. Chem. Soc.* **2012**, *134*, 12912−5.

(19) Probst, N.; Madarász, Á; Valkonen, A.; Pápai, I.; Rissanen, K.; Neuvonen, A.; et al. Cooperative Assistance in Bifunctional Organocatalysis: Enantioselective Mannich Reactions with Aliphatic and Aromatic Imines. *Angew. Chem. Int. Ed.* **2012**, *51*, 8495−9.

(20) Kennedy, C. R.; Lehnherr, D.; Rajapaksa, N. S.; Ford, D. D.; Park, Y.; Jacobsen, E. N. Mechanism-Guided Development of a Highly Active Bis-thiourea Catalyst for Anion-Abstraction Catalysis. *J. Am. Chem. Soc.* **2016**, *138*, 13525−8.

(21) Park, Y.; Harper, K. C.; Kuhl, N.; Kwan, E. E.; Liu, R. Y.; Jacobsen, E. N. Macrocyclic bis-thioureas catalyze stereospecific glycosylation reactions. *Science.* **2017**, *355*, 162−6.

(22) Pupo, G.; Ibba, F.; Ascough, D. M. H.; Vicini, A. C.; Ricci, P.; Christensen, K. E.; et al. Asymmetric nucleophilic fluorination under hydrogen bonding phase-transfer catalysis. *Science.* **2018**, *360*, 638−42.

(23) Ibba, F.; Pupo, G.; Thompson, A. L.; Brown, J. M.; Claridge, T. D. W.; Gouverneur, V. Impact of Multiple Hydrogen Bonds with Fluoride on Catalysis: Insight from NMR Spectroscopy. *J. Am. Chem. Soc.* **2020**, *142*, 19731−44.

(24) Wåhlander, J.; Amedjkouh, M.; Balcells, D. A DFT Perspective on Diels-Alder Organocatalysts Based on Substituted Phosphoramides: A DFT Perspective on Diels-Alder Organocatalysts Based on Substituted Phosphoramides. *Eur. J. Org. Chem.* **2019**, *2019*, 442−50.

(25) Sakai, N.; Kawashima, K.; Kajitani, M.; Mori, S.; Oriyama, T. Combined Computational and Experimental Studies on the Asymmetric Michael Addition of α-Aminomaleimides to β-Nitrostyrenes Using an Organocatalyst Derived from *Cinchona* Alkaloid. *Org. Lett.* **2021**, *23*, 5714−8.

(26) Zhu, J. L.; Zhang, Y.; Liu, C.; Zheng, A. M.; Wang, W. Insights into the Dual Activation Mechanism Involving Bifunctional Cinchona Alkaloid Thiourea Organocatalysts: An NMR and DFT Study. *J. Org. Chem.* **2012**, *77*, 9813−25.

(27) Wei, S.; Yalalov, D. A.; Tsogoeva, S. B.; Schmatz, S. New highly enantioselective thiourea-based bifunctional organocatalysts for nitro-Michael addition reactions. *Catal. Today.* **2007**, *121*, 151−7.

(28) Vazquez-Chavez, J.; Luna-Morales, S.; Cruz-Aguilar, D. A.; Díaz-Salazar, H.; Vallejo Narváez, W. E.; Silva-Gutiérrez, R. S.; et al. The effect of chiral *N* -substituents with methyl or trifluoromethyl groups on the catalytic performance of mono- and bifunctional thioureas. *Org. Biomol Chem.* **2019**, *17*, 10045−51.

(29) Hamza, A.; Schubert, G.; Soós, T.; Pápai, I. Theoretical Studies on the Bifunctionality of Chiral Thiourea-Based Organocatalysts: Competing Routes to C−C Bond Formation. *J. Am. Chem. Soc.* **2006**, *128*, 13151−60.

(30) Izzo, J. A.; Myshchuk, Y.; Hirschi, J. S.; Vetticatt, M. J. Transition state analysis of an enantioselective Michael addition by a bifunctional thiourea organocatalyst. *Org. Biomol Chem.* **2019**, *17*, 3934−9.

(31) Fukui, K. Theory of orientation and stereoselection. In *Orientation and Stereoselection*; Fukui, K, Ed.; Springer, Berlin; 1970; pp 1−85 (Fortschritte der Chemischen Forschung).

(32) Emamian, S.; Lu, T.; Kruse, H.; Emamian, H. Exploring Nature and Predicting Strength of Hydrogen Bonds: A Correlation Analysis Between Atoms-in-Molecules Descriptors, Binding Energies, and

Energy Components of Symmetry-Adapted Perturbation Theory. *J. Comput. Chem.* **2019**, *40*, 2868−81.
(33) Johnson, E. R.; Keinan, S.; Mori-Sánchez, P.; Contreras-García, J.; Cohen, A. J.; Yang, W. Revealing Noncovalent Interactions. *J. Am. Chem. Soc.* **2010**, *132*, 6498−506.
(34) Murray, J. S.; Brinck, T.; Lane, P.; Paulsen, K.; Politzer, P. Statistically-based interaction indices derived from molecular surface electrostatic potentials: a general interaction properties function (GIPF). *J. Mol. Struct THEOCHEM.* **1994**, *307*, 55−64.
(35) Hartke, B. Global optimization. *WIREs Comput. Mol. Sci.* **2011**, *1*, 879−87.
(36) Frisch, M. J.; Trucks, G. W.; Schlegel, H. B.; Scuseria, G. E.; Robb, M. A.; Cheeseman, J. R. et al. *Gaussian 16 Rev. C.01*; Gaussian, Inc.: Wallingford, CT; 2016.
(37) Hohenberg, P.; Kohn, W. Inhomogeneous Electron Gas. *Phys. Rev.* **1964**, *136*, B864−71.
(38) Kohn, W.; Sham, L. J. Self-Consistent Equations Including Exchange and Correlation Effects. *Phys. Rev.* **1965**, *140*, A1133−8.
(39) Salahub, D. R., Zerner, M. C., Eds. *The Challenge of d and f Electrons: Theory and Computation*; American Chemical Society, Washington, DC; 1989; ACS Symposium Series, Vol. *394*.
(40) Yang, W.; Parr, R. G. *Density functional theory of atoms and molecules*; Oxf Univ Press, 1989; Vol. *1*, p 989.
(41) Becke, A. D. Density-functional thermochemistry. I. The effect of the exchange-only gradient correction. *J. Chem. Phys.* **1992**, *96*, 2155−60.
(42) Becke, A. D. Density-functional thermochemistry. II. The effect of the Perdew−Wang generalized-gradient correlation correction. *J. Chem. Phys.* **1992**, *97*, 9173−7.
(43) Becke, A. D. Density-functional thermochemistry. III. The role of exact exchange. *J. Chem. Phys.* **1993**, *98*, 5648−52.
(44) Grimme, S. Semiempirical GGA-type density functional constructed with a long-range dispersion correction. *J. Comput. Chem.* **2006**, *27*, 1787−99.
(45) Grimme, S.; Antony, J.; Ehrlich, S.; Krieg, H. A consistent and accurate *ab initio* parametrization of density functional dispersion correction (DFT-D) for the 94 elements H-Pu. *J. Chem. Phys.* **2010**, *132*, 154104.
(46) Grimme, S.; Ehrlich, S.; Goerigk, L. Effect of the damping function in dispersion corrected density functional theory. *J. Comput. Chem.* **2011**, *32*, 1456−65.
(47) Hariharan, P. C.; Pople, J. A. The influence of polarization functions on molecular orbital hydrogenation energies. *Theor Chim Acta.* **1973**, *28*, 213−22.
(48) Clark, T.; Chandrasekhar, J.; Spitznagel, G. W.; Schleyer, P. V. R. Efficient diffuse function-augmented basis sets for anion calculations. III. The 3-21+G basis set for first-row elements, Li−F. *J. Comput. Chem.* **1983**, *4*, 294−301.
(49) Marenich, A. V.; Cramer, C. J.; Truhlar, D. G. Universal Solvation Model Based on Solute Electron Density and on a Continuum Model of the Solvent Defined by the Bulk Dielectric Constant and Atomic Surface Tensions. *J. Phys. Chem. B* **2009**, *113*, 6378−96.
(50) Hrivnák, T.; Budzák, Š; Reis, H.; Zaleśny, R.; Carbonnière, P.; Medved', M. Electric properties of hydrated uracil: From micro- to macrohydration. *J. Mol. Liq.* **2019**, *275*, 338−46.
(51) Thicoipe, S.; Carbonniere, P.; Pouchan, C. DFT modelling of the infrared spectra for isolated and aqueous forms of adenine. *Theor. Chem. Acc.* **2017**, *136*, 44.
(52) Carbonniere, P.; Thicoipe, S.; Pouchan, C. Theoretical Strategy to Build Structural Models of Microhydrated Inorganic Systems for the Knowledge of Their Vibrational Properties: The Case of the Hydrated Nitrate Aerosols. *J. Phys. Chem. A* **2013**, *117*, 3826−34.
(53) Thicoipe, S.; Carbonniere, P.; Pouchan, C. The Use of the GSAM Approach for the Structural Investigation of Low-Lying Isomers of Molecular Clusters from Density-Functional-Theory-Based Potential Energy Surfaces: The Structures of Microhydrated Nucleic Acid Bases. *J. Phys. Chem. A* **2013**, *117*, 7236−45.
(54) Witte, J.; Neaton, J. B.; Head-Gordon, M. Push it to the limit: Characterizing the convergence of common sequences of basis sets for intermolecular interactions as described by density functional theory. *J. Chem. Phys.* **2016**, *144*, 194306.
(55) Burns, L. A.; Mayagoitia, ÁV; Sumpter, B. G.; Sherrill, C. D. Density-functional approaches to noncovalent interactions: A comparison of dispersion corrections (DFT-D), exchange-hole dipole moment (XDM) theory, and specialized functionals. *J. Chem. Phys.* **2011**, *134*, 084107.
(56) Lefebvre, C.; Rubez, G.; Khartabil, H.; Boisson, J. C.; Contreras-García, J.; Hénon, E. Accurately extracting the signature of intermolecular interactions present in the NCI plot of the reduced density gradient versus electron density. *Phys. Chem. Chem. Phys.* **2017**, *19*, 17928−36.
(57) Bader, R. F. W. Atoms in Molecules. *A Quantum Theory*; Oxford University Press: New York, 1990.
(58) Bader, R. F. W. The Quantum Mechanical Basis of Conceptual Chemistry. *Monatshefte Für Chem. - Chem. Mon.* **2005**, *136*, 819−54.
(59) KUMAR, P. S. V.; RAGHAVENDRA, V.; SUBRAMANIAN, V. Bader's Theory of Atoms in Molecules (AIM) and its Applications to Chemical Bonding. *J. Chem. Sci.* **2016**, *128*, 1527−36.
(60) Lu, T.; Chen, F. Multiwfn: A multifunctional wavefunction analyzer. *J. Comput. Chem.* **2012**, *33*, 580−92.
(61) Foster, J. P.; Weinhold, F. Natural hybrid orbitals. *J. Am. Chem. Soc.* **1980**, *102*, 7211−8.
(62) Reed, A. E.; Weinhold, F. Natural bond orbital analysis of near-Hartree−Fock water dimer. *J. Chem. Phys.* **1983**, *78*, 4066−73.
(63) Reed, A. E.; Weinhold, F. Natural localized molecular orbitals. *J. Chem. Phys.* **1985**, *83*, 1736−40.
(64) Reed, A. E.; Weinstock, R. B.; Weinhold, F. Natural population analysis. *J. Chem. Phys.* **1985**, *83*, 735−46.
(65) Carpenter, J. E. Extension of Lewis structure concepts to open-shell and excited-state molecular species Ph.D. Thesis. University of Wisconsin, 1987.
(66) Naaman, R, Vager, Z, Ed. *The Structure of Small Molecules and Ions [Internet]*; Springer US: Boston, MA, 1988. Available from: http://link.springer.com/10.1007/978-1-4684-7424-4.
(67) Reed, A. E.; Curtiss, L. A.; Weinhold, F. Intermolecular interactions from a natural bond orbital, donor-acceptor viewpoint. *Chem. Rev.* **1988**, *88*, 899−926.
(68) Carpenter, J. E.; Weinhold, F. Analysis of the geometry of the hydroxymethyl radical by the "different hybrids for different spins" natural bond orbital procedure. *J. Mol. Struct THEOCHEM* **1988**, *169*, 41−62.

https://doi.org/10.1021/acs.joc.2c00562
J. Org. Chem. XXXX, XXX, XXX−XXX